Rheological, Thermal, and Chemical Evaluation of Asphalt Binders Modified Using Crumb Rubber and Warm-Mix Additive

K. Lakshmi Roja[1]; Mohammad Fuad Aljarrah[2]; Okan Sirin, Aff.M.ASCE[3];
Nasser Al-Nuaimi[4]; and Eyad Masad, F.ASCE[5]

Abstract: This study evaluates the potential of producing warm-mix asphalt (WMA) using a wax-based additive (Sasobit) in a binder modified using crumb rubber (CR). This binder is formulated for very hot climates and has a grade of PG 82E-16. Three proportions of Sasobit were added to the binder (1%, 2%, and 3%). In the compaction temperature range (130°C–145°C), there was 9% to 16% reduction in viscosity as a result of using 2% and 3% Sasobit. With an increased content of Sasobit, a higher dynamic modulus was identified for the 3% CR+Sasobit binder, and the rutting resistance of the binder also improved. From the fatigue tests, the use of 3% Sasobit caused noticeable reduction in fatigue life. From the nanoscale characterization conducted using Atomic Force Microscope (AFM), an island-type structure was observed for Sasobit-treated binders. This structure could be the wax crystalline phase that improved the stiffness of the binder in nano and macroscales. In addition, thermal analysis was carried out under endothermic and exothermic conditions. The binder's melting temperature reduced and the crystallization temperature increased with the addition of Sasobit. The CR+3% Sasobit binder had the highest percentage of the Carbonyl group, which is associated with binder aging and thus reduced the fatigue life. Overall, it was observed that Sasobit (up to an addition of a 2% dosage) improved the modulus and rutting resistance without degrading the cracking resistance of binders. **DOI: 10.1061/(ASCE)MT.1943-5533.0004194.** © *2022 American Society of Civil Engineers.*

Introduction

Large quantities of vehicle tires pile up every year in the State of Qatar. According to the Qatar Statistics Authority (Nunoo and Al-Tamimi 2020), a minimum of 500,000 scrap tires are disposed of every year. Therefore, there have been efforts in Qatar to develop engineering solutions for the use of tire rubber including the modification of asphalt binder.

Asphalt modification using crumb tire rubber started in the 1960s in Arizona (McDonald 1981). Consequently, research was carried out to produce stabilized rubber asphalt binders (Roberts et al. 1989; Choubane et al. 1999). The addition of rubber replaces the asphalt binder content by 15%–25%, and also improves the high and low-temperature performance of binders (rutting and fatigue) (Presti et al. 2012; Mashaan and Karim 2013; Jamal and Giustozzi 2020).

In the State of Qatar, the use of CR in asphalt binders started about five years ago to produce binders with high temperature grades (PG76-22 and PG 82-16). The modification of asphalt using CR requires high mixing temperatures (175°C), which is associated with high fuel consumption as well as undesirable environmental and work conditions. The use of WMA additive reduces the mix production temperatures of asphalt binders/mixtures by 20°C–30°C (D'Angelo et al. 2007; Bonaquist 2011; SABITA 2011; Al Mamun et al. 2020). Warm-mix technology has been gaining attention due to its ability to reduce mix production temperatures (reduce emissions), save fuel cost, and allow longer hauling distances during transportation of mix to the worksite (Hurley and Prowell 2005, 2006; Sadeq et al. 2018).

Sasobit is a warm-mix additive that is produced from the Fischer–Tropsch process. This wax-based additive contains longer aliphatic hydrocarbon chains. The congealing point of Sasobit is approximately 100°C–110°C (Sasolwax 2016). Above the congealing point, it completely melts in the binder, and below this temperature it forms a robust crystalline structure. When using WMA technologies, the additive not only reduces the mix production temperatures but also influences the material performance properties. Hence, it is necessary to select an optimum dosage of WMA additive without negatively affecting the asphalt performance properties.

A few researchers (Wang et al. 2012; Kök et al. 2014; Julaganti et al. 2017; Gong et al. 2019) have tried to benefit from Sasobit by using it as a WMA additive for polymer-modified binder (PMB) and CR binder. In general, the PMB is heated around 175°C during the mix production, and the compaction temperature could be around 145°C. For every 10°C reduction in the mix production temperatures, the fuel oil savings could be at least 1 L/t mix, and the CO_2 emission could be reduced by 1 kg/t mix (Krambeck 2009). Prior to adding Sasobit to the binder, an in-depth investigation is required to determine its impact at the mix production temperature

[1]Assistant Research Scientist, Mechanical Engineering Program, Texas A&M Univ. at Qatar, P.O. Box 23874, Doha, Qatar (corresponding author). ORCID: https://orcid.org/0000-0003-1862-7293. Email: lakshmi.kakumanu@qatar.tamu.edu

[2]Graduate Research Assistant, Zachry Dept. of Civil and Environmental Engineering, Texas A&M Univ., College Station, TX 77843. ORCID: https://orcid.org/0000-0002-6643-8721. Email: m.aljarrah@tamu.edu

[3]Associate Professor, Dept. of Civil and Architectural Engineering, Qatar Univ., P.O. Box 2713, Doha, Qatar. Email: okansirin@qu.edu.qa

[4]Director, Center for Advanced Materials, Qatar Univ., P.O. Box 2713, Doha, Qatar. Email: anasser@qu.edu.qa

[5]Professor, Mechanical Engineering Program, Texas A&M Univ. at Qatar, P.O. Box 23874, Doha, Qatar. Email: eyad.masad@qatar.tamu.edu

© ASCE   04022049-1   J. Mater. Civ. Eng.

J. Mater. Civ. Eng., 2022, 34(5): 04022049

regime and the pavement service temperature regime. In addition, thermal and chemical analyses give insights about the impact of adding Sasobit on the binder composition and its impact on the rheological properties. Considering these aspects in this study, the objectives are framed as follows:

- Evaluate the potential use of Sasobit in reducing the mix production temperatures of crumb rubber (CR)–modified binder that has high grade (PG82E);
- Determine the effect of using Sasobit on the performance grade and rheological properties of CR binders;
- Investigate the rutting and fatigue response of CR+Sasobit asphalt binders at their critical temperatures;
- Characterize the nanomechanical properties of CR+Sasobit binders and relate these properties to the performance and optimum content of Sasobit;
- Analyze the thermal properties of Sasobit treated rubber binders to understand their impact on the rheological properties; and
- Evaluate the aging resistance of CR+Sasobit binders by determining their chemical properties.

Materials & Methodology

In this study, a binder modified with CR was used, which has a PG grade of PG 82E-16. A wax-based WMA additive (Sasobit) was added to the binder in three different dosages (1%, 2%, and 3%). These dosages were selected based on the recommendations in the literature (Hurley and Prowell 2005; Liu et al. 2011; Jamshidi et al. 2012).

The CR asphalt binder was heated at 150°C for 1.5 h, and the Sasobit was blended in the binder at a speed of 1,000 rpm for 30 min. The binders in different aging conditions were used for testing, i.e., unaged, short-term, and long-term aged. The short- and long-term aging of the binders were conducted by following the ASTM D2872-04 (ASTM 2004) and ASTM D6521-13 (ASTM 2013a) procedures, respectively. Short-term aging was carried out at 163°C for 85 min in a rolling thin film oven (RTFO). Long-term aging was carried at 110°C for 20 h in a pressure aging vessel (PAV) with an air pressure of 2.1 ± 0.1 MPa. The experimental methodology for all binders is given in Fig. 1.

Rheological Properties at Mixing and Compaction Temperatures Regime

To measure the influence of Sasobit on the asphalt binder viscosity, a steady shear rotational viscosity tests were carried at temperatures of 175°C, 160°C, 145°C, 130°C, and 115°C. The spindle's speed was selected so that the machine torque limit was maintained around 50%. The selected spindle speeds were 90, 70, 50, 20, and 5 at temperatures 175°C, 160°C, 145°C, 130°C, and 115°C, respectively. At temperatures ≤145°C, the CR binder and CR+Sasobit binders were sheared for 1,800 s. However, at temperatures ≥160°C, the shearing duration was 1,200 s. The first 600 s were considered presharing, and viscosity measurements were recorded after presharing as shown in Fig. 2. At each temperature, two trials were conducted for each material. The mean viscosity values and the percentage error from the mean are shown in Fig. 2. At temperatures above 130°C, the percentage error was less than 3.5%, [ASTM D4402 (ASTM 2013b)] and the viscosity curves below 130°C have error percentages less than 5% from their mean.

At high temperatures (≥130°C), Sasobit significantly reduced binder viscosity [Figs. 2(a and b)]. However, the trend was completely reversed at 115°C as the binder's viscosity increased with an increase in Sasobit dosage [Fig. 2(c)]. This is attributed to Sasobit forming crystalline structures at a temperature close to its congealing point (Sasolwax 2016; Jamshidi et al. 2012, 2013), which, in turn, increases the viscosity/stiffness at these temperatures.

For all the binders, the viscosity at the 1,200th second was summarized and plotted in Fig. 3. The temperature corresponding to the viscosity value of 3 Pascal second (Pa·s) was compared for CR asphalt binder and CR+Sasobit binders. With the equi-viscous approach, only a 4°C reduction in the temperature was detected for 3% Sasobit–treated binders [Fig. 3(a)]. In other words, while there is a significant decrease in Sasobit-treated binders' viscosity values, this phenomenon is not reflected as a significant temperature reduction. A similar finding was reported in other studies (Wasiuddin et al. 1998; Bennert et al. 2010; You et al. 2011; Simone et al. 2012). Bennert et al. (2010) cautioned that the equi-viscous criteria might not work for WMA binders. It is only suitable for unmodified HMA binders. Hence, the actual viscosity
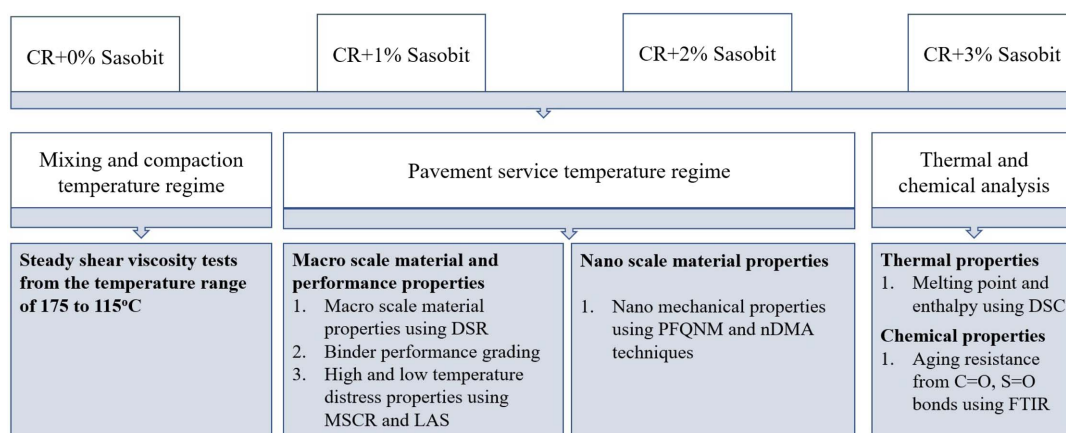
CR- crumb rubber modified binder; RV- rotational viscometer; DSR- dynamic shear rheometer; PFQNM- peak force quantitative nanomechanical mapping; nDMA- nano dynamic mechanical analysis; MSCR- multiple stress creep and recovery; LAS- linear amplitude sweep; DSC: Differential scanning calorimetry; FTIR: Fourier-transform infrared spectroscopy

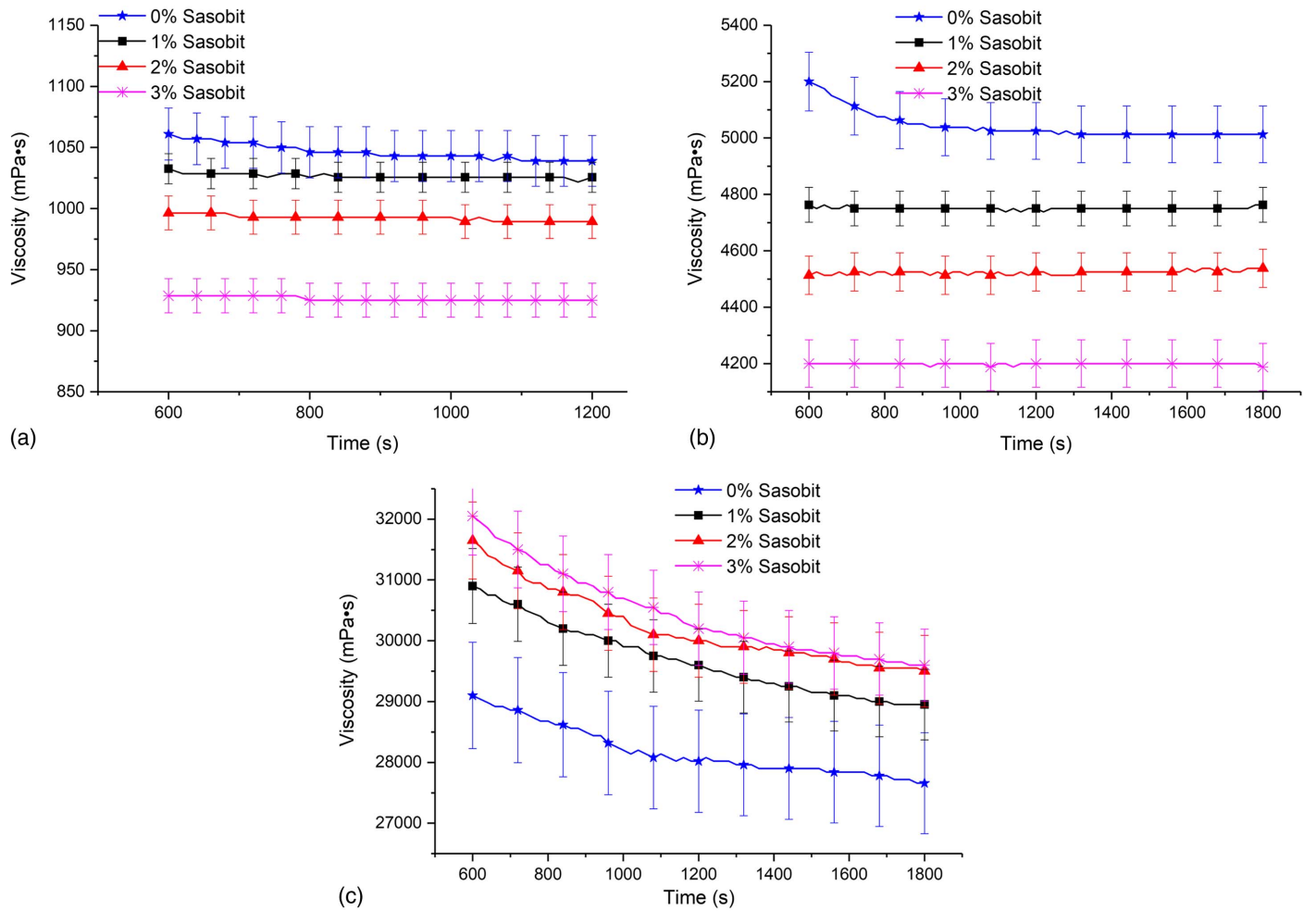**Fig. 1.** Experimental methodology.

Fig. 2. Steady shear viscosity at different temperatures: (a) 160°C; (b) 130°C; and (c) 115°C.
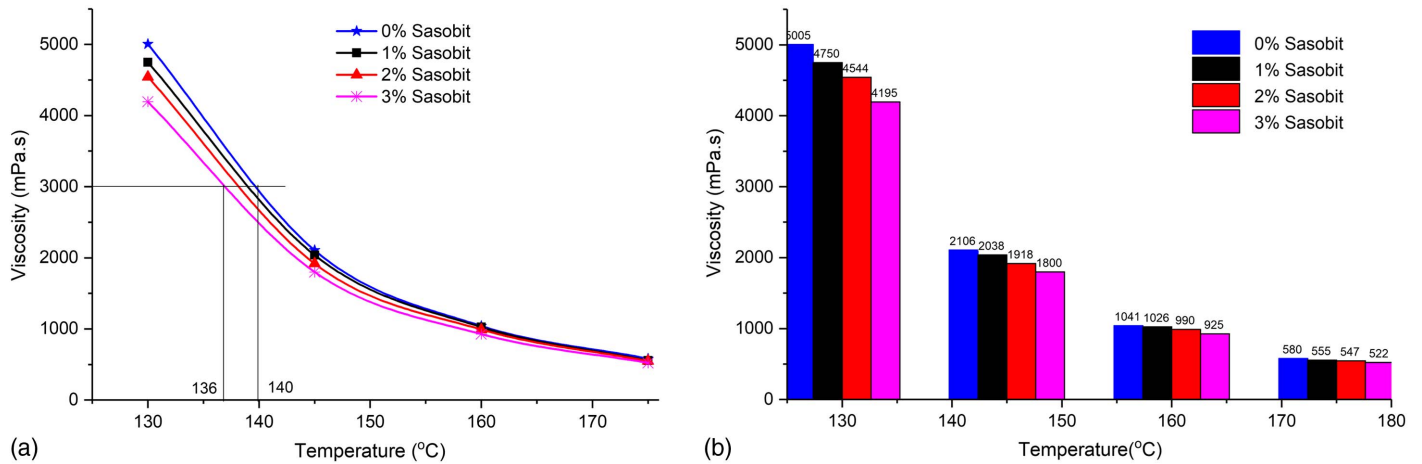

Fig. 3. Viscosity reduction with the addition of Sasobit at different temperatures: (a) equi-viscous approach; and (b) viscosity values.

reduction (%) with the addition of Sasobit was measured from the corresponding control CR asphalt binder. These values are shown in Fig. 3(b) at each temperature. Within the compaction temperature range (145°C–130°C), a significant reduction in viscosity (9% to 16.2%) was found for 2% and 3% Sasobit–treated binders. These results show that the compaction temperatures of CR+Sasobit binders can be lowered than the conventional asphalt binder. The use of 1% Sasobit content may not be effective in reducing the mix

production temperatures for the high-grade binder (PG 82E) used in this present study.

Performance Grading [AASHTO M 332-14 (AASHTO 2014)]

In this test, high and intermediate critical temperatures were measured using a dynamic shear rheometer (DSR) and low critical

© ASCE   04022049-3   J. Mater. Civ. Eng.

J. Mater. Civ. Eng., 2022, 34(5): 04022049

temperatures were determined using a bending beam rheometer (BBR). These values are tabulated in Table 1. The addition of Sasobit increased the PG high temperature and did not adversely influence the low-temperature grade.

The values of the rutting parameter ($G^*/\sin\delta$) were compared for all CR+Sasobit binders at 82°C in Fig. 4. At pavement service temperatures, the addition of Sasobit increased the dynamic modulus and decreased the phase angle. Although the addition of Sasobit

Table 1. Performance grading of binders

| Test	0% Sasobit	1% Sasobit	2% Sasobit	3% Sasobit
PG high: original ($G^*/\sin\delta$), kPa				
88	1.4	2.52	2.95	3.62
94	0.91	1.77	2.05	2.53
100	—	1.09	1.27	1.52
106	—	0.61	0.64	0.76
PG high (continuous)	93	101	103	105
PG high: RTFO ($G^*/\sin\delta$), kPa				
82	3.17	3.79	5.38	7.3
88	2.06	2.57	3.66	4.95
94	—	1.69	2.75	3.25
100	—	—	1.71	2.08
PG high (continuous)	87	91	97	99
PG intermediate: PAV ($G^* \times \sin\delta$), kPa				
28	3,060	2,840	3,000	3,780
25	4,370	4,180	4,350	5,330
22	6,210	6,070	6,230	7,970
PG intermediate (continuous)	24	24	24	26
BBR (stiffness ≤ 300 MPa, $m \geq 0.3$)				
Stiffness at −6°C	96.8	98.4	102	123
Slope at −6°C	0.346	0.365	0.327	0.312
Stiffness at −12°C	195	195	218	219
Slope at −12°C	0.297	0.29	0.29	0.253
BBR pass/fail temperature	−6	−6	−6	−6
PG low	−16	−16	−16	−16
MSCR, J_{nr}, kPa^{-1}				
J_{nr} 3.2 kPa at 82°C	0.414	0.0993	0.0739	0.0685
PG grade	PG82-16	PG88-16	PG94-16	PG94-16
Common PG grade	PG82E-16	PG82E-16	PG82E-16	PG82E-16
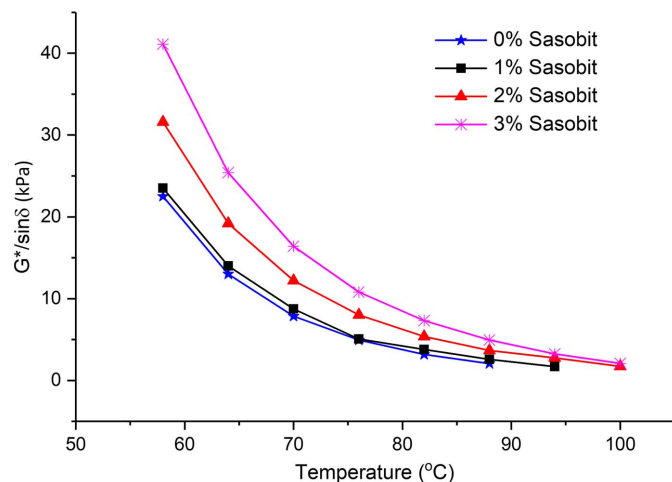
Fig. 4. $G^*/\sin\delta$ at different temperatures.

increased the BBR stiffness at -6°C, the values were far less than 300 MPa, and the slope values were greater than 0.3 (see Fig. 5, Table 1). The traffic grade was assigned based on the J_{nr} value. All the binders have J_{nr} values less than 0.5 kPa^{-1} at 82°C, and a traffic grade of E was assigned.

Viscoelastic Properties: Dynamic Shear Rheometer

For measuring binder viscoelastic properties, the frequency sweep test was carried out using a DSR at different frequency and temperature ranges. In this test, a sinusoidal waveform is applied, the modulus is calculated from the peak stress and strain, and the phase angle is calculated from the time lag between stress-strain curves.

The test temperatures were 25°C, 35°C, 45°C, 55°C, 65°C; at each temperature, frequency sweep was applied starting from 15 to 1 Hz (1 Hz/s). At pavement service temperatures (25°C–65°C), the addition of Sasobit increased the dynamic moduli and reduced the phase angle of the binder. Using the time-temperature superposition principle (TTSP), the obtained temperature isotherms were shifted to a reference temperature (T_{ref}) of 21°C (Fig. 6). Eqs. (1) and (2) were used for finding the coefficients of shift factors (a_1 and a_2) and master curves (b_1, b_2, b_3, and b_4), respectively (Jameson 2006)

$$log(a(T)) = a_1(T^2 - T_{ref}^2) + a_2(T - T_{ref}) \quad (1)$$

$$log(|G^*|) = b_1 + \frac{b_2}{1 + exp(-b_3 - b_4 log(f_R))} \quad (2)$$

The shift factors are shown in Table 2. The binders with 2% and 3% Sasobit content exhibited more temperature sensitivity than 0% and 1% Sasobit binders. This is evident from the coefficients of shift factors and master curves (Table 2). A similar result was reported for Sasobit-treated binders in the studies carried out by Liu et al. (2010) and Roja et al. (2016).

Rutting Resistance: Creep and Recovery Tests

To characterize the rutting resistance of binders, creep and recovery tests were conducted. First, the standard multiple stress creep and recovery (MSCR) test was conducted at two small stress levels of 0.1 and 3.2 kPa. Ten creep and recovery cycles were applied with 1-s loading and 9-s rest periods at each stress level. As described in ASTM D7405-20 (ASTM 2020), the nonrecoverable creep compliance (J_{nr}) was determined at each stress level. It was observed that the Sasobit binders have lower J_{nr} values compared to plain rubber binder, the J_{nr} values at 3.2 kPa stress level were 0.414, 0.100, 0.074, and 0.069 kPa^{-1} for 0%, 1%, 2%, and 3% Sasobit–treated binders, respectively.

In recent studies (Vajipeyajula et al. 2020; Atul Narayan et al. 2015; Roja et al. 2018), researchers reported that the magnitude of standard stress levels and the rest duration periods may not be sufficient to capture material behavior. Hence, in this study, the binders were subjected to repeated creep and recovery cycles (RCRMS) at multiple stress levels of 0.1, 3.2, 6.4, 9.6, 12.8 kPa and rest periods of 9, 20, 50, 70, and 150 s, respectively. From the strain accumulation of plain CR and Sasobit-treated binders, the J_{nr} values are calculated. For checking repeatability, a minimum of two tests were conducted for each material, and the mean J_{nr} and standard deviation are shown in Fig. 7. The J_{nr} versus recovery (%) at 3.2 kPa is plotted in Fig. 8. When the dosage of Sasobit increased from 1% to 2%, the binder recovery (%) increased from 89.5% to 96%, whereas the recovery only increased from 96% to 96.7%
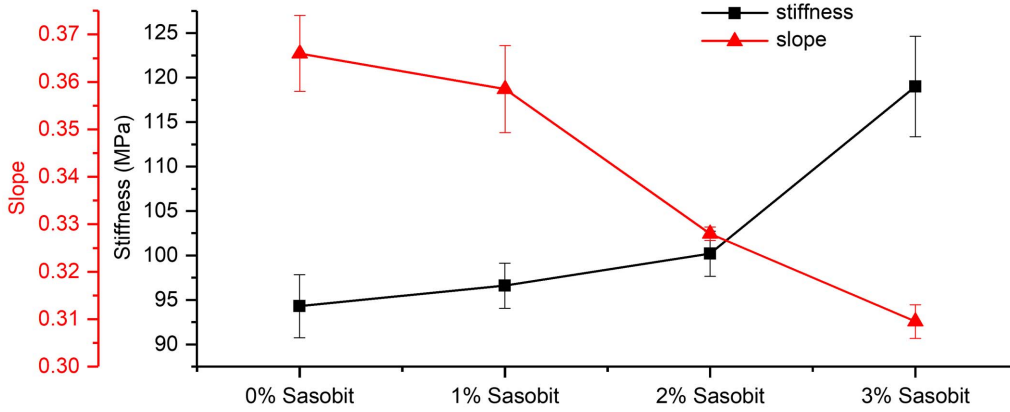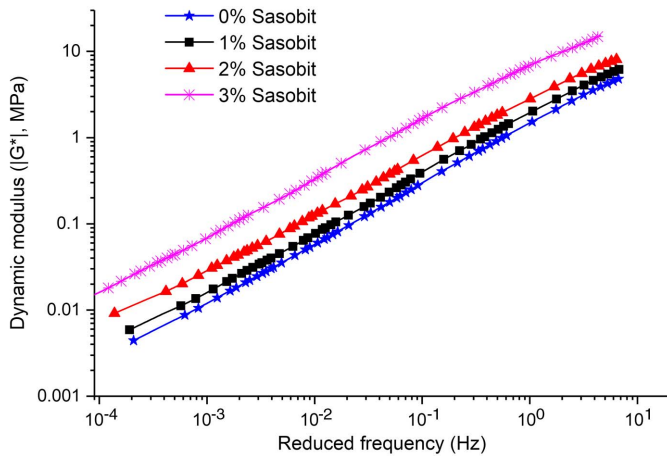
© ASCE 04022049-4 J. Mater. Civ. Eng.

J. Mater. Civ. Eng., 2022, 34(5): 04022049

Fig. 5. BBR stiffness at $-6°C$.

Fig. 6. Master curves constructed at 21°C.

Fig. 7. Nonrecoverable creep compliance values obtained from RCRMS test.

Table 2. Coefficients of shift factors and master curves for Sasobit-treated binders

Materials	a_1	a_2	b_1	b_2	b_3	b_4
0% Sasobit	0.000787	−0.1511	1.547	7.302	0.5445	0.3925
1% Sasobit	0.000737	−0.1477	2.086	6.490	0.6073	0.4432
2% Sasobit	0.000802	−0.1565	2.486	6.017	0.6575	0.4600
3% Sasobit	0.000854	−0.1622	2.496	6.039	0.9359	0.4640

when the Sasobit content changed from 2% to 3%. This shows that there is no much added value in improving the binder recovery by adding Sasobit higher than 2%.

When longer rest periods were used to allow binders to recover, the J_{nr} values decreased, and the J_{nr} comparison of MSCR and RCRMS tests are shown in Fig. 9 at 3.2 kPa. Even at a very high-stress level of 12.8 kPa, the 3% Sasobit–treated binder has a low J_{nr} value of 1.241 kPa^{-1}, which indicates V traffic grade, whereas plain CR binder has an S grade [as per AASHTO M 332-14 (AASHTO 2014)]. For all the binders, the J_{nr} difference between 9.6 and 12.8 kPa was less than 50% (33%–47%), representing the least stress sensitivity of such binders.

Fatigue Response: Linear Amplitude Strain Sweep Test

The number of cycles for fatigue failure can be determined using the linear amplitude sweep (LAS) test [AASHTO TP 101-14
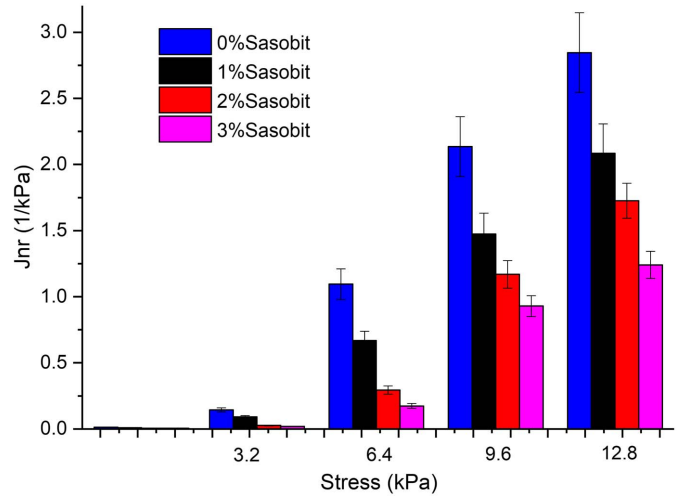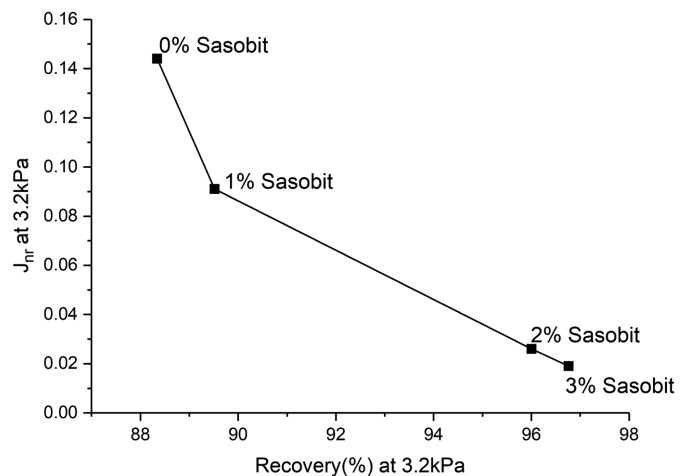

Fig. 8. J_{nr} versus recovery (%) at 3.2 kPa in RCRMS test.

(AASHTO 2013)]. In the standard test protocol, the strain sweep test is conducted in continuation of the frequency sweep test. As per AASHTO TP 101-14 (AASHTO 2013), the strain value shall linearly increase from 0% to 30% in 3,100 s (31,000 cycles at 10-Hz
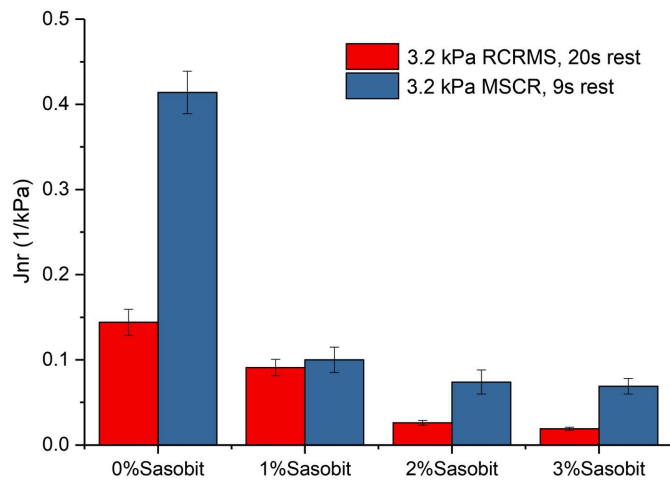
© ASCE 04022049-5 J. Mater. Civ. Eng.

J. Mater. Civ. Eng., 2022, 34(5): 04022049

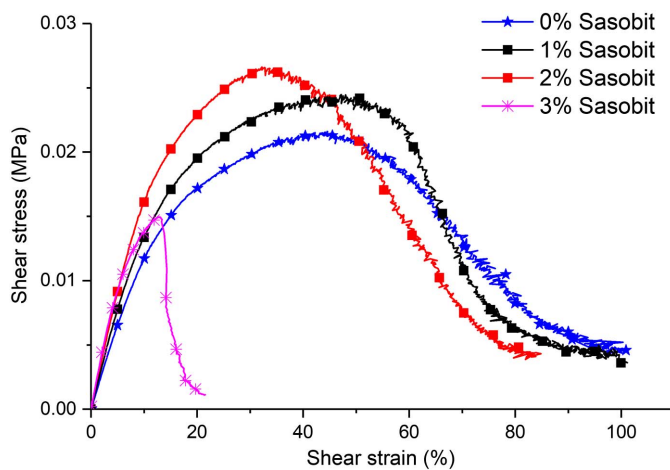**Fig. 9.** Influence of longer rest period on J_{nr} values at 3.2 kPa.

Fig. 10. Shear stress versus strain in LAS test.

frequency). Three replicates were tested for each PAV-aged binder. In this test, the plain CR binder did not fail within the test duration (within 30% strain). Hence, the test method was slightly modified by linearly increasing the strain value from 0% to 100% in 1,000 s (10,000 cycles at 10-Hz frequency). Fig. 10 shows the oscillatory shear stress curves for different dosages of CR+Sasobit binders. For 0%, 1%, 2%, and 3% Sasobit binders, the stress reached peak value at around 50%, 50%, 35%, and 15% strain values; after that, the stress started decreasing. The strain corresponding to peak stress values decreased with Sasobit dosage.

As given in AASHTO TP 101-14 (AASHTO 2013), fatigue life was determined using the viscoelastic continuum damage (VECD) approach. The failure point is defined when the oscillatory stress started decreasing. The fatigue failure cycles are calculated at

critical strain levels of 2.5%, 5%, and 10%. The mean values of all three replicates and their standard deviation are tabulated in Table 3. Although the binder's modulus increased significantly with the addition of 3% Sasobit content, the same binder failed early in less number of cycles compared to the other binders. The Sasobit dosage up to the addition of 2% did not significantly affect CR+Sasobit fatigue life.

AFM Measurements of Nanomechanical Properties

The nanoproperties of the binders were determined using two test protocols: peak force quantitative nanomechanical mapping (PFQNM) to characterize the nanomechanical properties, and nano-dynamic mechanical analysis (nDMA) to measure the nanoviscoelastic properties. In both protocols, the RTESPA-300-30 probe was used. This newly developed probe with a predetermined spring constant and tip radius values gives accurate measurements due to its larger signal-to-noise ratio (Dokukin and Sokolov 2012; Pittenger et al. 2019). Moreover, this probe is more appropriate for heterogeneous samples where the same peak force loading will yield different indentations for different materials, resulting in more accurate modulus values (Pittenger et al. 2010, 2019).

The binder samples were prepared using the heat and cast approach described in the study by Aljarrah and Masad (2020). The unaged CR+Sasobit binders were tested after 24 h of sample preparation. First, binder mechanical properties were captured using the PFQNM technique. Then, the nanoscale viscoelastic properties were determined using the nDMA technique at different temperatures and frequencies. The selected temperatures for both PFQNM and nDMA testing are 25°C, 35°C, and 45°C and are controlled using a low-drift heater. The detailed test procedure of PFQNM and nDMA techniques are explained in the following sections.

The Peak-Force Quantitative Nanomechanical Mapping (PFQNM) Test

The detailed principle of the PFQNM technique is illustrated in the study by Roja et al. (2020). In this test, as the tip starts moving towards the sample surface, attraction forces emerge (electrostatic or Van Der Waals forces). Afterward, the tip touches the sample surface and applies a compressive force until the "peak force" value is reached. Finally, the tip retracts from the surface where the compressive force decreases to zero then switches to a tensile force (below the x-axis). The maximum negative force value represents the adhesion force between the sample surface and the tip.

Plotting force versus tip-sample separation curve assists in finding the nanomechanical properties of the sample. The PFQNM test enables observing samples' surface topography and calculating their Derjaguin, Muller, Toropov (DMT) (Derjaguin et al. 1975) modulus value simultaneously with Nanoscope software. To find the DMT elastic modulus, the linear part of the retraction (withdrawal) curve is fitted against the DMT mechanical model (Derjaguin et al. 1975, 1994; Maugis 2013) as shown in Eq. (3)

Table 3. Number of fatigue failure cycles

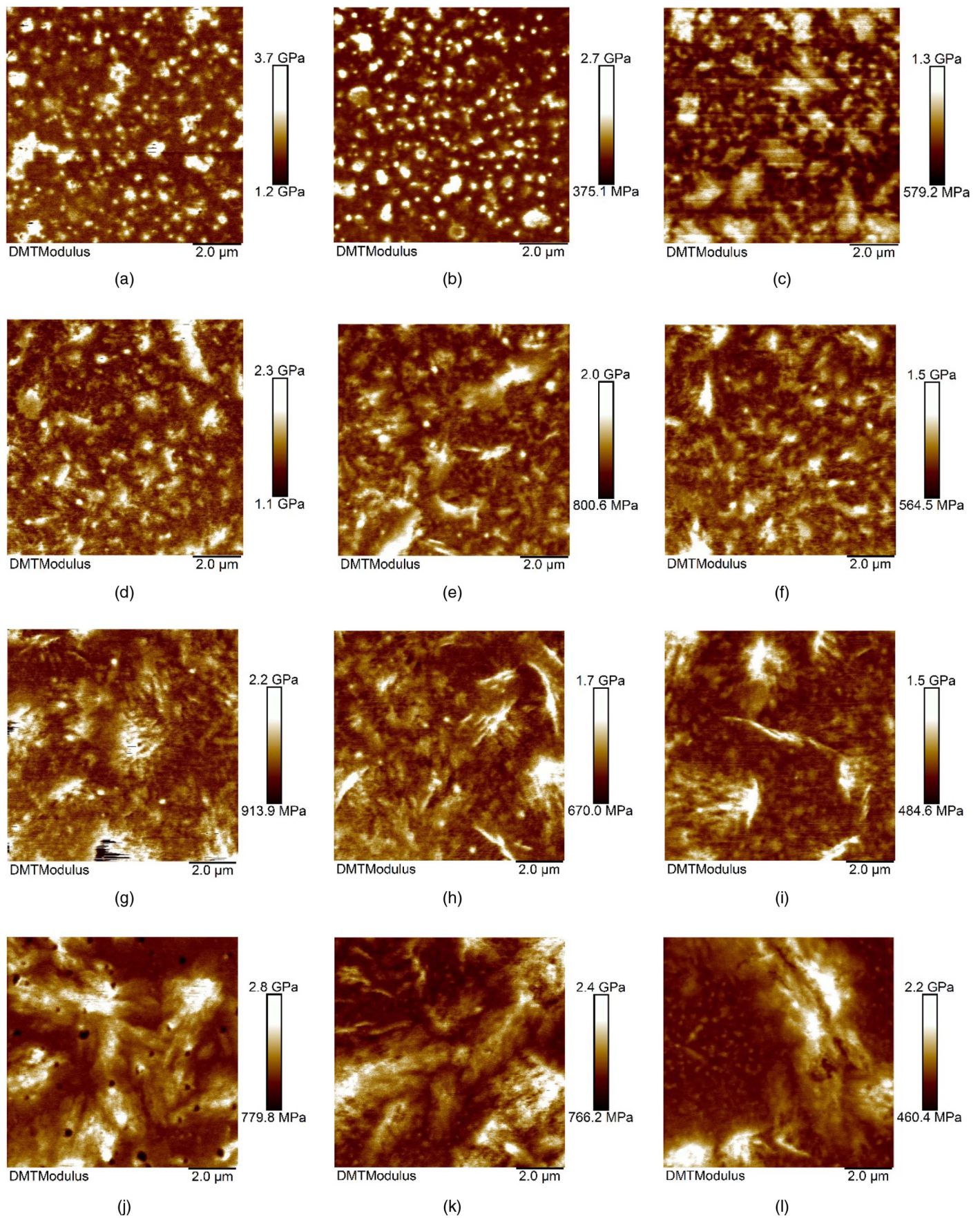| Strain (%)	0% Sasobit		1% Sasobit		2% Sasobit		3% Sasobit	
	Mean	SD	Mean	SD	Mean	SD	Mean	SD
2.5	1.75×10^7	4.38×10^6	1.42×10^7	3.12×10^6	1.40×10^7	2.80×10^6	1.18×10^5	2.01×10^4
5	1.35×10^6	3.38×10^5	9.67×10^5	2.13×10^5	9.55×10^5	1.91×10^5	5.90×10^3	1.00×10^3
10	1.03×10^5	2.58×10^4	6.58×10^4	1.45×10^4	6.50×10^4	1.30×10^4	2.96×10^2	5.03×10^1

Fig. 11. DMT modulus maps of CR and CR+Sasobit–treated rubber asphalt binders: (a) 0% Sasobit, 25℃; (b) 0% Sasobit, 35℃; (c) 0% Sasobit, 45℃; (d) 1% Sasobit, 25℃; (e) 1% Sasobit, 35℃; (f) 1% Sasobit, 45℃; (g) 2% Sasobit, 25℃; (h) 2% Sasobit, 35℃; (i) 2% Sasobit, 45℃; (j) 3% Sasobit, 25℃; (k) 3% Sasobit, 35℃; and (l) 3% Sasobit, 45℃.

© ASCE 04022049-7 J. Mater. Civ. Eng.

J. Mater. Civ. Eng., 2022, 34(5): 04022049

$$F - F_{Adh} = \frac{4}{3} E^* \sqrt{R\delta^3} \qquad (3)$$

where F = peak force value; F_{Adh} = adhesive force; R = tip radius; δ = sample deformation; and E^* = reduced DMT modulus.

In the PFQNM test, the images were captured at a scan size of $10 \times 10 \ \mu m$, with a scan rate of 0.5 Hz, and the resolution was 480×480. The selected peak force was 100 nN with a frequency of 1 kHz. The selected probe has a tip radius of 31 nm and the spring constant was 48.23 N/m. Fig. 11 shows the DMT modulus maps. Large radius tips capture nanomechanical properties better than sharp tips (Dokukin and Sokolov 2012; Pittenger et al. 2019). As can be seen for the 0% Sasobit control sample at all testing temperatures (Fig. 11), CR distribution across the binder phase resembles the shape of separate islands. As the temperature increased, CR particles started to connect and congregate, as seen at the 45°C temperature. However, the use of Sasobit had a significant impact on CR distribution across the binder phase, where even for 1% dosage, the islands started to connect. The connected islands are more prominent when the dosage of Sasobit increased in the blend. In a study conducted by Gong et al. (2019), the rubber and Sasobit particle distribution was measured using a laser scanning confocal microscope and identified better homogeneity of blend with the addition of Sasobit.

To further explore the homogeneity of the blends, statistical analysis for DMT modulus distribution was carried out. Two measures of variability, namely, the coefficient of variance (COV) and interquartile range (IQR) for each sample, were calculated. The COV is the ratio of the image standard deviation to the mean, and the IQR is the difference between the 75th and the 25th percentiles of the DMT values. The values are listed in Table 4. Among these binders, the 0% Sasobit–treated binder had the highest variability. This high variability of 0% Sasobit (CR binder) hinders depicting a trend in DMT mean values. When Sasobit is added to the binder, it formed crystalline structures between rubber and asphalt binder; the least variability was seen for 1% Sasobit binders. Again, at high Sasobit dosages (3%), the high variability was seen due to the interconnected island structures formed on the binder's surface. Hence, the optimum dosage of Sasobit could be between 1% and 2%. In addition, as can be seen in Fig. 11 and Table 4, temperature sensitivity decreased as Sasobit dosage increased, where the drop in DMT modulus values decreased with an increase in temperature. For example, the 1%-Sasobit sample DMT values dropped from 1,763 to 1,087 to 846 MPa for 25°C, 35°C, and 45°C, respectively, while for 3% Sasobit, the drop went from 1,551 to 1,382 to 1,034 MPa for 25°C, 35°C, and 45°C, respectively. From the nanoscale measurements, the least temperature susceptibility was noticed for the 3% Sasobit, whereas the 3%-Sasobit binders exhibited the highest temperature susceptibility at the macroscale (Table 2).

Table 4. Samples variability measures (COV, IQR)

Sample, temperature	Mean (MPa)	Sd (MPa)	COV (%)	IQR (MPa)
0% Sasobit, 25°C	1,983	351	18	297
0% Sasobit, 35°C	1,036	307	30	224.4
0% Sasobit, 45°C	869	113	13	156.4
1% Sasobit, 25°C	1,763	154	9	191.6
1% Sasobit, 35°C	1,087	92.7	9	108.7
1% Sasobit, 45°C	846	77.4	9	94.8
2% Sasobit, 25°C	1,401	181	13	198.5
2% Sasobit, 35°C	1,048	137	13	149.9
2% Sasobit, 45°C	821	136	17	133.1
3% Sasobit, 25°C	1,551	292	19	357.1
3% Sasobit, 35°C	1,382	239	17	312.1
3% Sasobit, 45°C	1,034	242	23	272

The reasons for the differences in temperature susceptibility at different scales are not well understood from these results.

Nanoscale Dynamic Mechanical Analysis (nDMA) test

The nDMA test is utilized to capture the nanoscale viscoelastic properties and is conducted following the PFQNM test. In nDMA, a small magnitude of peak force (<20 nN) was applied without damaging the sample. Many preliminary trials were conducted to select the peak force based on the tip radius and deformation of the bitumen samples. For all bitumen samples, the deformation values were <10 nm, which is usually considered as a linear regime for measuring material properties in nanoscale. A detailed description of the test procedure is given in Aljarrah and Masad (2020), Aljarrah et al. (2021), and Pittenger et al. (2019). Initially, the tip applies a preloading force until it touches the sample surface. Then, a relaxation period takes place to eliminate the sample's creep. Afterward, force modulation occurs at the selected frequencies. Finally, the tip retracts from the surface, where the adhesion force is calculated. The test outputs are the axial modulus ($|E^*|$) and phase angle (δ). The following equation was used to convert the axial modulus into a shear modulus, which is most common in binder rheology

$$|E^*| = 2|G^*|(1 + \upsilon^*) \qquad (4)$$

where υ = Poisson's ratio [0.5 for incompressible fluids as given by Gudmarsson et al. (2015)]. In this study, frequency sweeps ranging between 1 and 30 Hz were carried out at different temperatures of 25°C, 35°C, and 45°C. Sweeps were conducted on 40 different locations on each sample to check the repeatability of test results.

Fig. 12 shows the frequency sweep test data of CR+Sasobit binders at 25°C, 35°C, and 45°C, respectively. As can be seen from the figures, there is no specific trend in the $|G^*|/\sin(\delta)$ curves of binders. It should be realized that the nDMA test is conducted on a further finer scale than the PFQNM test because the latter can produce images at a $10-\mu m$ scale, and the former is performed at a maximum of tens of nanometers scales (depending on the contact area between the sample and tip). In DSR, the bulk sample was tested between parallel plates, the variation in the properties of small individual particles was not accounted for whereas in AFM, the sample was subjected to loading in the nano/microlevel. The tip measured the properties of individual particles (bitumen, rubber, and wax) in the bitumen. At such a fine testing scale, different constituents with different properties are detected (as seen in Fig. 11). The $|G^*|/\sin(\delta)$ values showed in Fig. 12 are the average of all particles. This is the reason for seeing large variations in material properties.

Except for 0% Sasobit, the $|G^*|/\sin(\delta)$ parameter increased as Sasobit dosage increased. The nDMA results are in line with the PFQNM test results in terms of temperature sensitivity; as Sasobit dosage increased, the temperature sensitivity decreased. For example, for 1% Sasobit, at a frequency of 30 Hz, the $|G^*|/\sin(\delta)$ parameter decreased from 140 to 90 to 50 MPa at 25°C, 35°C, and 45°C, respectively. On the other hand, the values decreased from 190 to 130 to 100 MPa at 25°C, 35°C, and 45°C, respectively, for the 3%-Sasobit binder.

Thermal Analysis

Thermal analysis was performed using differential scanning calorimetry via a DSC 8500 (Perkin Elmer, USA). In this test, the samples were heated from 20°C to 150°C and cooled back to 20°C for two cycles at a heating rate of 10°C per min under a Nitrogen atmosphere at a flow rate of 40 mL/min.
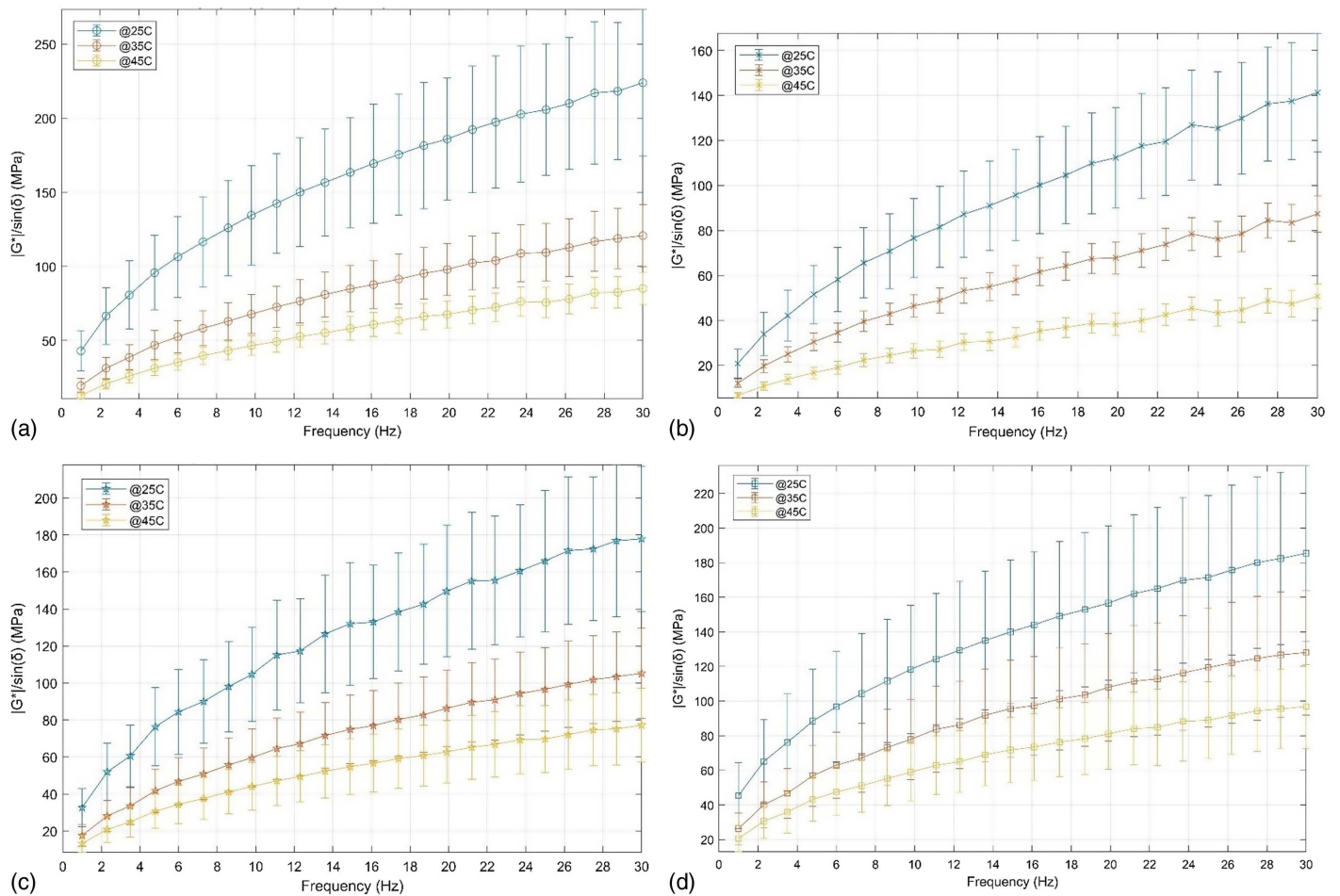
© ASCE   04022049-8   J. Mater. Civ. Eng.

J. Mater. Civ. Eng., 2022, 34(5): 04022049

Fig. 12. $|G^*|/\sin\delta|$ values across different frequencies and temperatures: (a) frequency sweeps for 0%-Sasobit binder (CR binder); (b) frequency sweeps for 1% CR+Sasobit binder; (c) frequency sweeps for 2% CR+Sasobit binder; and (d) frequency sweeps for 3% CR+Sasobit binder.
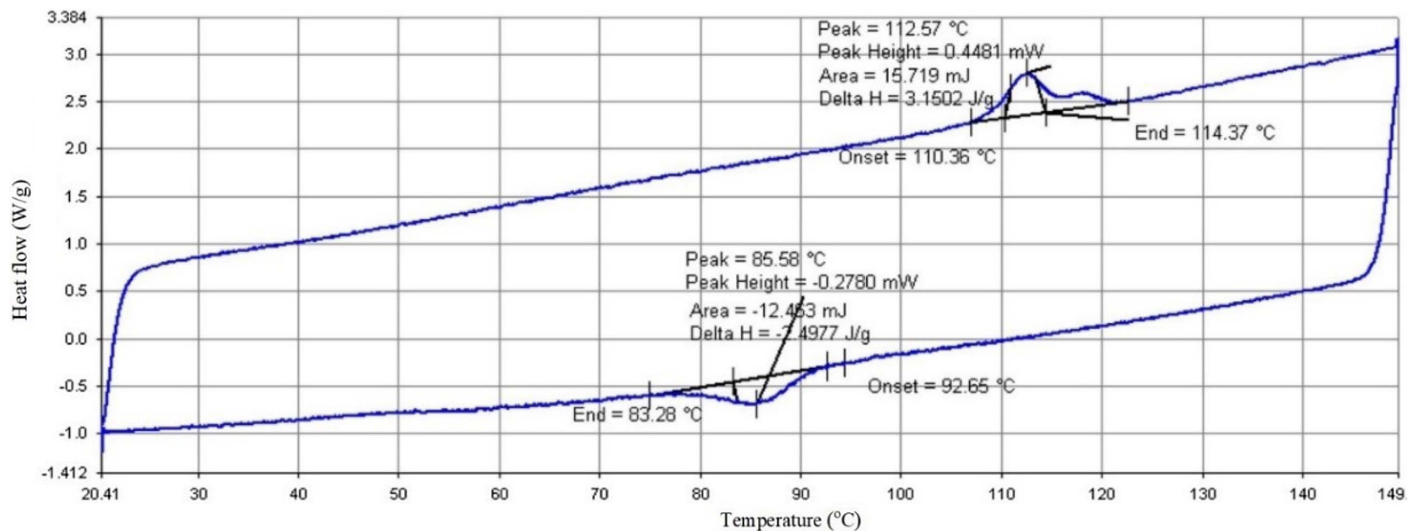

Fig. 13. Heat flow curve during endotherm and exotherm modes for 3% PAV-aged CR+Sasobit binder.

The DSC results are used to determine the melting point, and crystallization transition temperatures. The heat flow curves are used to calculate the enthalpies of transitions; the enthalpy is an area under peak that is calculated by integrating the peak corresponding to a given transition. The melting point of the material is obtained from the endothermic peak, and the crystallization is measured from the exothermic peak.

During the endothermic condition, the sample absorbs heat to show the transition from solid to liquid and the sample release heat during the exothermic process when crystallization occurs. The

Table 5. Melting, crystallization temperatures, and enthalpy data obtained from DSC analysis

Material	Endotherm		Exotherm	
	Peak	ΔH (J/g)	Peak	ΔH (J/g)
Unaged				
0% Sasobit	117.91	1.579	No peak	No peak
1% Sasobit	114.06	2.435	77.37	2.069
2% Sasobit	113.45	3.275	79.96	3.14
3% Sasobit	113.35	3.000	82.32	3.387
PAV-aged				
0% Sasobit	117.56	1.355	56.03	0.175
1% Sasobit	112.84	2.135	79.88	1.723
2% Sasobit	112.64	2.778	84.21	2.443
3% Sasobit	112.57	3.150	85.58	2.497

enthalpy change (ΔH) is positive when the energy absorbs during the endothermic process, whereas it is negative when the material releases energy during the exothermic condition (Lukas and LeMaire 2009).

The heat flow curve of the 3% PAV–aged Sasobit binder is shown in Fig. 13. The peaks in endotherm (heating) and exotherm (cooling) modes were identified for all the binders and listed in Table 5. The endotherm peak represents the melting point, and the exotherm peak represents the crystallization of samples.

For all the binders, the melting point was identified to be between 112°C and 118°C, and the crystallization occurred between 55°C and 86°C. The binder without Sasobit had no peak in the exothermic condition (the plain rubber binder has negligible crystallinity), whereas a small peak was identified for the same binder after long-term aging condition. The addition of Sasobit reduced the binder's melting temperature and started crystallizing early at higher temperatures in exothermic conditions. For example, as the dosage of Sasobit increased from 0% to 3%, the melting point of binder reduced from 117.91°C to 113.35°C, and the peak crystallization temperature increased from 77.37°C to 82.32°C for 1% to 3% Sasobit binders, respectively. While the crystallization temperatures increased with the long-term aging condition, binders' melting temperatures were not affected much. The crystallization in the plain rubber binder could be the attribution of asphaltene content, whereas in the Sasobit treated binder, it could be due to the binder asphaltene content and Sasobit wax (Sellers 2009).

The heat of fusion (enthalpy, ΔH) is the area under endothermic and exothermic peak curves. In exothermic conditions, the area under peak curves increased with the Sasobit dosage. Because the Sasobit cocrystallized with asphaltene content of binder, this enhanced the performance of total blend (Sellers 2009). This could be the reason for higher moduli of Sasobit-treated binders at pavement service temperatures.

Chemical Analysis

Chemical analysis was performed using a Fourier Transform Infrared spectrometer (FTIR) Frontier MIR model (Perkin Elmer, USA) at a 4 cm^{-1} resolution in the scan range of $4000 - 500$ cm^{-1} in the attenuated total reflection (ATR) mode with a ZnSe crystal plate.

The carbonyl and sulfoxide peaks were identified for all PAV-aged binders (Figs. 14 and 15). The area under these peaks was used in calculating carbonyl and sulfoxide index. Carbonyl index ($I_{c=o}$) is the ratio of area under $C = O$ peak (1,700 cm^{-1}) to the sum of ethylene and methyl peaks at 1,460 and 1,375 cm^{-1}, respectively. Sulfoxide index ($I_{s=o}$) is the ratio of area under $S = O$ peak (1,030 cm^{-1}) to the sum of ethylene and methyl peaks. The obtained values are listed in Table 6. The $I_{c=o}$ and $I_{s=o}$ values increased with
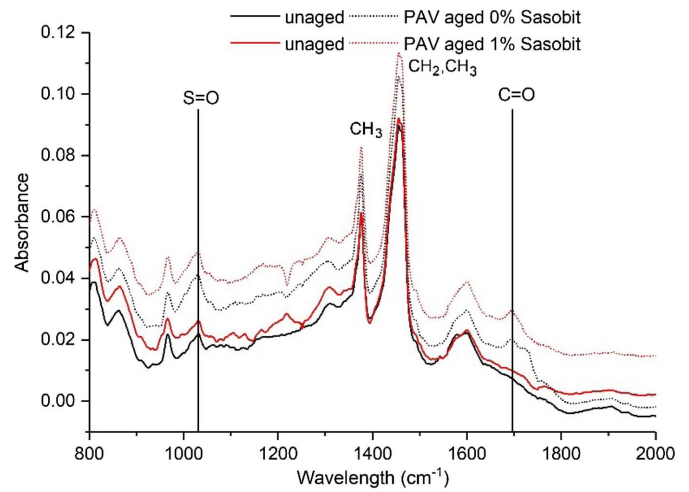

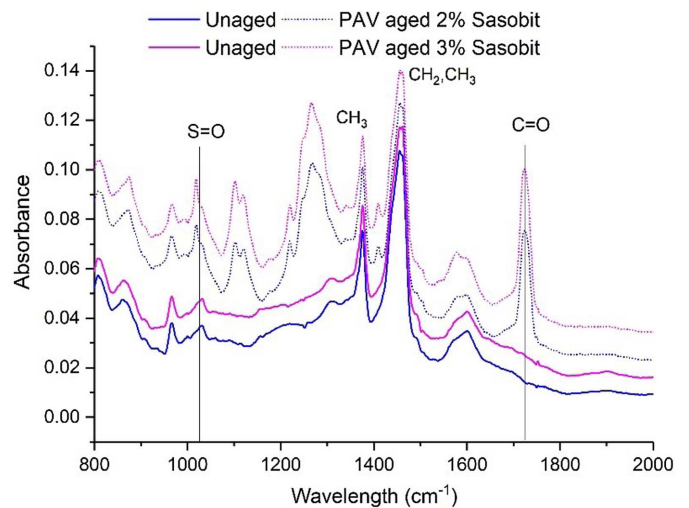**Fig. 14.** Absorbance spectra for 0%, 1% Sasobit–treated binders.

Fig. 15. Absorbance spectra for 2%, 3% Sasobit–treated binders.

Table 6. Area of peaks, carbonyl, and sulfoxide index values

Material	$C = O$ 1,700 cm^{-1}	$S = O$ 1,030 cm^{-1}	CH$_3$ 1,375 cm^{-1}	CH$_2$, CH$_3$ 1,460 cm^{-1}	Carbonyl Index	Sulfoxide Index
0% Sasobit PAV	0.243	0.129	0.545	2.553	0.078	0.041
1% Sasobit PAV	0.573	0.148	0.614	2.553	0.18	0.046
2% Sasobit PAV	0.781	0.136	0.538	2.273	0.277	0.048
3% Sasobit PAV	1.108	0.182	0.491	2.240	0.405	0.066

Sasobit content, and the 3% Sasobit–treated binder has a very high carbonyl index of 0.405. This highly aged binder negatively impacted the 3%-Sasobit binder's cracking resistance and resulted in the shortest fatigue life in the LAS test. Hence, the optimum Sasobit dosage of 2% was recommended from this study based on the binders' rheology, performance, thermal, and chemical properties.

Conclusions

This study was motivated by the need to develop sustainable asphalt binders that incorporate recycled materials and require less

energy consumption for its mixing and compaction. Consequently, this study provides characterization of asphalt binders modified using crumb rubber (CR) and Sasobit at mixing, compaction, and pavement service temperatures. The viscosity of CR+Sasobit binders was measured at the mixing and compaction temperature. It was found that the addition of 2% and more of Sasobit significantly reduced CR binder viscosity. This can allow better workability and more compaction time of CR+Sasobit binders.

The addition of Sasobit increased the performance grading high temperature to 94°C without negatively impacting the low temperature properties. The viscoelastic properties measured using the DSR showed that Sasobit increased binder stiffness at service temperatures.

The nonrecoverable creep compliance decreased with the addition of Sasobit. The J_{nr} difference for the stress levels of 9.4 and 12.8 kPa was observed to be between 33% and 47% for all the binders. The addition of Sasobit did not significantly influence the stress sensitivity of asphalt binders. Moreover, the use of up to 2% Sasobit did not significantly affect the binder fatigue resistance, whereas the 3% Sasobit binder failed early due to the brittleness of the binder.

The nanoscale characterization using the AFM showed that the addition of Sasobit changed the binder's microstructure by forming interconnected islands in the binder. These formations were associated with an increase in the binder's overall stiffness. Based on the nanoscale measurements, the optimum dosage of Sasobit for CR binders used in this study is around 1% to 2% because this range helped to increase stiffness and at the same time had less variability in the modulus than the 3% CR+Sasobit binder.

From the thermal analysis, the melting temperatures of binders decreased with the addition of Sasobit. These results agree with the viscosity measurements using steady shear experiments. In exothermic conditions, Sasobit cocrystallized with asphaltene content of binder, which improved the stiffness of the blend.

The carbonyl and sulfoxide index values increased for long-term aged CR+Sasobit binders. The degraded fatigue performance of the 3% Sasobit–treated binder could be due to the significant increase in the Carbonyl index.

To conclude, the optimum percentage of Sasobit is 2% for the CR binder used in this study (PG 82E). This percentage improved the modulus and rutting resistance of the binder without adversely affecting its cracking resistance. Moreover, the thermal and chemical characterization of the blends supported the use of this percentage of Sasobit.

Data Availability Statement

Some or all data, models, or code that support the findings of this study are available from the corresponding author upon reasonable request (experimental and analytical results).

Acknowledgments

References

AASHTO. 2013. *Estimating damage tolerance of asphalt binders using the linear amplitude sweep*. AASHTO TP 101-14. Washington, DC: AASHTO.

AASHTO. 2014. *Specification for performance based asphalt binder using multiple stress creep recovery (MSCR) test*. AASHTO M 332-14. Washington, DC: AASHTO.

Aljarrah, M., K. L. Roja, E. Masad, M. Ouederni, and O. B. Ibikunle. 2021. "Nanostructural and Nanomechanical Properties of LDPE Modified Binders." *J. Mater. Civ. Eng*.

Aljarrah, M. F., and E. Masad. 2020. "Nanoscale viscoelastic characterization of asphalt binders using the AFM-nDMA test." *Mater. Struct.* 53 (4): 1–15. https://doi.org/10.1617/s11527-020-01543-3.

Al Mamun, A., O. Sirin, and E. Masad. 2020. "Development of warm mix asphalt with the aid of microstructural characterization." In *Proc., Int. Conf. on Civil Infrastructure and Construction (CIC 2020)*, 273–280. Doha, Qatar: Qatar University Press.

ASTM. 2004. *Standard test method for effect of heat and air on a moving film of asphalt (rolling thin-film oven test)*. ASTM D2872-04. West Conshohocken, PA: ASTM.

ASTM. 2013a. *Standard practice for accelerated aging of asphalt binder using a pressurized aging vessel (PAV)*. ASTM D6521-13. West Conshohocken, PA: ASTM.

ASTM. 2013b. *Standard test method for viscosity determination of asphalt at elevated temperatures using a rotational viscometer*. ASTM D4402. West Conshohocken, PA: ASTM.

ASTM. 2020. *Standard test method for multiple stress creep and recovery (MSCR) of asphalt binder using a dynamic shear rheometer*. ASTM D7405-20. West Conshohocken, PA: ASTM.

Atul Narayan, S., D. N. Little, and K. R. Rajagopal. 2015. "Analysis of rutting prediction criteria using a nonlinear viscoelastic model." *J. Mater. Civ. Eng.* 27 (3): 04014137. https://doi.org/10.1061/(ASCE)MT.1943-5533.0001078.

Bennert, T., G. Reinke, W. Mogawer, and K. Mooney. 2010. "Assessment of workability and compactability of warm–mix asphalt." *Transp. Res. Rec.* 2180 (1): 36–47. https://doi.org/10.3141/2180-05.

Bonaquist, R. F. 2011. *Vol. 702 of Precision of the dynamic modulus and flow number tests conducted with the asphalt mixture performance tester*. Washington, DC: Transportation Research Board.

Choubane, B., G. A. Sholar, J. A. Musselman, and G. C. Page. 1999. "Ten-year performance evaluation of asphalt-rubber surface mixes." *Transp. Res. Rec.* 1681 (1): 10–18. https://doi.org/10.3141/1681-02.

D'Angelo, J., R. Kluttz, R. N. Dongre, K. Stephens, and L. Zanzotto. 2007. "Revision of the superpave high temperature binder specification: The multiple stress creep recovery test." *J. Assoc. Asphalt Paving Technol.* 76: 123–162.

Derjaguin, B., V. Muller, and Y. P. Toporov. 1994. "Effect of contact deformations on the adhesion of particles." *Prog. Surf. Sci.* 45 (1–4): 131–143. https://doi.org/10.1016/0079-6816(94)90044-2.

Derjaguin, B. V., V. M. Muller, and Y. P. Toporov. 1975. "Effect of contact deformations on the adhesion of particles." *J. Colloid Interface Sci.* 53 (2): 314–326. https://doi.org/10.1016/0021-9797(75)90018-1.

Dokukin, M. E., and I. Sokolov. 2012. "Quantitative mapping of the elastic modulus of soft materials with HarmoniX and PeakForce QNM AFM modes." *Langmuir* 28 (46): 16060–16071. https://doi.org/10.1021/la302706b.

Gong, J., Y. Liu, Q. Wang, Z. Xi, J. Cai, G. Ding, and H. Xie. 2019. "Performance evaluation of warm mix asphalt additive modified epoxy asphalt rubbers." *Constr. Build. Mater.* 204 (Apr): 288–295. https://doi.org/10.1016/j.conbuildmat.2019.01.197.

Gudmarsson, A., N. Ryden, H. Di Benedetto, and C. Sauzeat. 2015. "Complex modulus and complex poisson's ratio from cyclic and dynamic modal testing of asphalt concrete." *Constr. Build. Mater.* 88 (Jul): 20–31. https://doi.org/10.1016/j.conbuildmat.2015.04.007.

Hurley, G. C., and B. D. Prowell. 2005. *Evaluation of sasobit for use in warm mix asphalt*. Rep. No. NCAT report 05-06. Auburn, AL: Auburn Univ.

Hurley, G. C., and B. D. Prowell. 2006. *Evaluation of evotherm for use in warm mix asphalt*. Rep. No. NCAT report 06-02. Auburn, AL: Auburn Univ.

Jamal, M., and F. Giustozzi. 2020. "Low-content crumb rubber modified bitumen for improving australian local roads condition." *J. Cleaner Prod.* 271 (Oct): 122484. https://doi.org/10.1016/j.jclepro.2020.122484.

© ASCE   04022049-11   J. Mater. Civ. Eng.

J. Mater. Civ. Eng., 2022, 34(5): 04022049

Jameson, G. 2006. *Guide to pavement technology: Part 2: Pavement structural design*. Rep. No AGPT02/08. Sydney, Australia: Austroads.

Jamshidi, A., M. O. Hamzah, and M. Y. Aman. 2012. "Effects of sasobit content on the rheological characteristics of unaged and aged asphalt binders at high and intermediate temperatures." *Mater. Res.* 15 (4): 628–638. https://doi.org/10.1590/S1516-14392012005000083.

Jamshidi, A., M. O. Hamzah, and Z. You. 2013. "Performance of warm mix asphalt containing sasobit: State-of-the-art." *Constr. Build. Mater.* 38 (Jan): 530–553. https://doi.org/10.1016/j.conbuildmat.2012.08.015.

Julaganti, A., R. Choudhary, and A. Kumar. 2017. "Rheology of modified binders under varying doses of WMA additive–sasobit." *Pet. Sci. Technol.* 35 (10): 975–982. https://doi.org/10.1080/10916466.2017.1297827.

Kök, B. V., M. Yılmaz, and M. Akpolat. 2014. "Evaluation of the conventional and rheological properties of SBS+ sasobit modified binder." *Constr. Build. Mater.* 63 (Jul): 174–179. https://doi.org/10.1016/j.conbuildmat.2014.04.015.

Krambeck, H. 2009. *Draft GHG emmissions calculator for asphalt production*. Washington, DC: World Bank.

Liu, J., S. Saboundjian, P. Li, B. Connor, and B. Brunette. 2011. "Laboratory evaluation of sasobit-modified warm-mix asphalt for Alaskan conditions." *J. Mater. Civ. Eng.* 23 (11): 1498–1505. https://doi.org/10.1061/(ASCE)MT.1943-5533.0000226.

Liu, Z., J. Wen, and S. Wu. 2010. "Influence of warm mix asphalt additive on temperature susceptibility of asphalt binders." In *Proc., 4th Int. Conf. on Bioinformatics and Biomedical Engineering*, 1–4. New York: IEEE.

Lukas, K., and P. K. LeMaire. 2009. "Differential scanning calorimetry: Fundamental overview." *Resonance* 14 (8): 807–817. https://doi.org/10.1007/s12045-009-0076-7.

Mashaan, N. S., and M. R. Karim. 2013. "Investigating the rheological properties of crumb rubber modified bitumen and its correlation with temperature susceptibility." *Mater. Res.* 16 (1): 116–127. https://doi.org/10.1590/S1516-14392012005000166.

Maugis, D. 2013. Vol. 130 of *Contact, adhesion and rupture of elastic solids*. New York: Springer.

McDonald, C. H. 1981. "Recollections of Early Asphalt-Rubber History." In *National seminar on asphalt-rubber*. Washington, DC: USDOT.

Nunoo, C. N., and S. A. Al-Tamimi. 2020. "Implementation of crumb rubber modified binder for Qatar local roads construction projects." In *Proc., Int. Conf. on Civil Infrastructure and Construction (CIC 2020)*, 403–412. Doha, Qatar: Qatar Univ.

Pittenger, B., N. Erina, and C. Su. 2010. *Quantitative mechanical mapping at the nanoscale with PeakForce QNM. Application Note AN128*. Plainview, NY: Veeco Instruments.

Pittenger, B., S. Osechinskiy, D. Yablon, and T. Mueller. 2019. "Nanoscale DMA with the atomic force microscope: A new method for measuring viscoelastic properties of nanostructured polymer materials." *JOM* 71 (10): 3390–3398. https://doi.org/10.1007/s11837-019-03698-z.

Presti, D. L., G. Airey, and P. Partal. 2012. "Manufacturing terminal and field bitumen-tyre rubber blends: The importance of processing conditions." *Procedia-Social Behav. Sci.* 53: 485–494. https://doi.org/10.1016/j.sbspro.2012.09.899.

Roberts, F. L., P. S. Kandhal, E. R. Brown, and R. L. Dunning. 1989. *Investigation and evaluation of ground tire rubber in hot mix asphalt*. NCAT Rep. No. 89-3. Auburn, AL: Auburn Univ.

Roja, K. L., E. Masad, B. Vajipeyajula, W. Yiming, E. Khalid, and V. C. Shunmugasamy. 2020. "Chemical and multi-scale material properties of recycled and blended asphalt binders." *Constr. Build. Mater.* 261 (Nov): 119689. https://doi.org/10.1016/j.conbuildmat.2020.119689.

Roja, K. L., A. Padmarekha, and J. M. Krishnan. 2018. "Rheological investigations on warm mix asphalt binders at high and intermediate temperature ranges." *J. Mater. Civ. Eng.* 30 (4): 04018038. https://doi.org/10.1061/(ASCE)MT.1943-5533.0002027.

Roja, K. L., N. Roy, and J. M. Krishnan. 2016. "Influence of aging on the rheological behavior of warm mix asphalt binders." In *Proc., 8th RILEM Int. Symp. on Testing and Characterization of Sustainable and Innovative Bituminous Materials*, 497–508. New York: Springer.

SABITA (Southern African Bitumen Association). 2011. *Best practice guideline for warm mix asphalt—Manual 32*. Cape Town, South Africa: SABITA.

Sadeq, M., E. Masad, H. Al-Khalid, O. Sirin, and L. Mehrez. 2018. "Linear and nonlinear viscoelastic and viscoplastic analysis of asphalt binders with warm mix asphalt additives." *Int. J. Pavement Eng.* 19 (10): 857–864. https://doi.org/10.1080/10298436.2016.1213592.

Sasolwax. 2016. *Sasobit redux-product information and summary of results*. Hamburg, Germany: Sasolwax.

Sellers, B. H. 2009. "Characterization and transitions of asphalt cement composite materials." M.S. thesis, Dept. of Chemistry, Louisiana State Univ.

Simone, A., M. Pettinari, F. Petretto, and A. Madella. 2012. "The influence of the binder viscosity on the laboratory short term aging." *Procedia Soc. Behav. Sci.* 53 (Oct): 421–431. https://doi.org/10.1016/j.sbspro.2012.09.893.

Vajipeyajula, B., K. L. Roja, E. Masad, and K. R. Rajagopal. 2020. "Analysis of reclaimed asphalt blended binders using linear and nonlinear viscoelasticity frameworks." *Mater. Struct.* 53 (5): 1–14. https://doi.org/10.1617/s11527-020-01554-0.

Wang, H., Z. Dang, Z. You, and D. Cao. 2012. "Effect of warm mixture asphalt (WMA) additives on high failure temperature properties for crumb rubber modified (CRM) binders." *Constr. Build. Mater.* 35 (Oct): 281–288. https://doi.org/10.1016/j.conbuildmat.2012.04.004.

Wasiuddin, N., S. Selvamohan, M. Zaman, and M. Guegan. 1998. "Comparative laboratory study of sasobit and aspha-min additives in warm-mix asphalt." *Transp. Res. Rec.* 1998 (1): 82–88. https://doi.org/10.3141/1998-10.

You, Z., S. W. Goh, and Q. Dai. 2011. *Laboratory evaluation of warm mix asphalt*. Rep. No. RC-1556. Houghton, MI: Michigan Technological Univ.

© ASCE

04022049-12

J. Mater. Civ. Eng.

J. Mater. Civ. Eng., 2022, 34(5): 04022049